

Puzzling Isotonic Odd-Even Staggering of Charge Radii in Deformed Rare Earth Nuclei

E. Takacs ,^{1,2} H. Staiger ,¹ S.A. Blundell ,³ N. Kimura ,² H.A. Sakaue ,² R.F. Garcia Ruiz ,⁴ W. Nazarewicz ,⁵ P.-G. Reinhard ,⁶ C.A. Faiyaz,¹ C. Suzuki ,² Dipti,¹ I. Angeli,⁷ Yu. Ralchenko ,^{8,9,10} I. Murakami ,² D. Kato ,^{2,11} Y. Nagai,¹² R. Takaoka,¹² Y. Miya ,¹² and N. Nakamura ,¹²

¹Department of Physics and Astronomy, Clemson University, Clemson, SC 29634

²National Institute for Fusion Science, Toki, Gifu 509-5292, Japan*

³Univ. Grenoble Alpes, CEA, CNRS, Grenoble INP, IRIG, SyMMES, 38000 Grenoble, France

⁴Massachusetts Institute of Technology, Cambridge, Massachusetts 02139

⁵Facility for Rare Isotope Beams and Department of Physics and Astronomy, Michigan State University, East Lansing, Michigan 48824

⁶Institut für Theoretische Physik II, Universität Erlangen-Nürnberg, Staudtstrasse 7, D-91058 Erlangen, Germany

⁷Department of Experimental Physics, University of Debrecen, Hungary, 4026

⁸Department of Astronomy, University of Maryland, College Park, MD 20742

⁹Astrophysics Science Division, NASA/GSFC, Greenbelt, MD 20771

¹⁰Center for Research and Exploration in Space Science and Technology, NASA/GSFC, Greenbelt, MD 20771

¹¹Interdisciplinary Graduate School of Engineering Sciences, Kyushu University, Fukuoka 816-8580, Japan

¹²Institute for Laser Science, The University of Electro-Communications, Tokyo 182-8585, Japan

The nuclear charge radius is a fundamental observable that encodes key aspects of nuclear structure, deformation, and pairing. Isotonic (constant neutron number) systematics in the deformed rare-earth region have long suggested that odd- Z nuclei are more compact than their even- Z neighbors—except for Lu, whose recommended radius appeared anomalously large relative to Yb and Hf. We report a high-precision determination of the natural-abundance-averaged Lu-Yb charge-radius difference using extreme-ultraviolet spectroscopy of highly charged Na-like and Mg-like ions, supported by high-accuracy relativistic atomic-structure calculations—a recently introduced method with the unique ability to measure inter-element charge radius differences. Combined with muonic-atom and optical isotope-shift data, our result resolves the longstanding Lu inversion anomaly and reestablishes a pronounced odd-even staggering along the $N = 94$ isotonic chain. The magnitude of this staggering is unexpectedly large, far exceeding that observed in semi-magic nuclei and in deformed isotopic sequences. State-of-the-art nuclear density functional theory calculations, including quantified uncertainties, fail to reproduce this enhancement, possibly indicating missing structural effects in current models. Our work demonstrates the power of highly charged ions for precise, element-crossing charge-radius measurements and provides stringent new constraints for future theoretical and experimental studies of nuclear-size systematics.

Introduction — The charge radius is a fundamental nuclear observable that encodes the spatial distribution of nucleons within the nucleus, and offers insight into many properties of finite nuclei and nuclear matter [1–7]. In heavy, deformed nuclei, measurements of charge radii provide key insights into how nuclear collectivity arises from the underlying shell structure [8–11]. These insights guide nuclear theory calculations, which are critical components of tests for beyond the Standard Model physics using isotope shifts [12, 13] and have been used in muonic-atom charge-radius measurements to estimate nuclear polarization effects [14, 15].

Our current understanding of how nuclear size evolves with proton and neutron number relies primarily on comparisons across isotopic (constant Z) chains that reveal striking variations in charge radii [16] and odd–even staggering (OESR) as a function of neutron number

N [17]. In contrast, systematic comparisons across isotonic chains (constant N) remain sparse, because commonly used techniques, such as laser spectroscopy [6], do not allow direct cross-element comparisons. This poses a major experimental obstacle to investigating the impact of isospin-breaking contributions and to constraining nuclear-matter properties using charge-radius measurements [18–22]. Hence, developing methods that allow robust comparisons of charge radii between different elements is a pressing need.

In this work, we employ extreme ultraviolet (EUV) spectroscopy of highly charged Na-like and Mg-like ions [23] to extract a high-precision difference in nuclear charge radii between naturally abundant Lu and Yb elements. When anchored to muonic atom data for Yb [24], our result provides an independent determination of the absolute nuclear charge radii of Lu isotopes, including ^{175}Lu [25].

By reducing previous uncertainties threefold, our measurement establishes a pronounced OES and resolves the longstanding Lu inversion anomaly [26]. In contrast, a dramatically reduced OES has been observed in both the

* Contacts: etakacs@clemson.edu, hstaiger@clemson.edu, kimura.naoki@nifs.ac.jp, n_nakamu@ils.uec.ac.jp

isotopic chains of deformed rare earth nuclei, and in isotopic and isotonic chains of heavy semi-magic nuclei. A reduced staggering has also been predicted by our state-of-the-art nuclear Density Functional Theory (DFT) calculations. To resolve this puzzle, precise measurements of charge radii of odd- Z deformed rare earth nuclei are called for. The experimental method used in this work provides a promising avenue for such investigations.

Atomic Structure Theory — The theoretical cornerstone of this work is the high precision attainable in atomic structure calculations for few-valence electron ions, achieved through relativistic many-body perturbation theory (RMBPT) with quantum electrodynamic (QED) corrections [27]. Focusing on transition energy differences, rather than individual transition energies, significantly reduces both experimental and theoretical uncertainties, allowing for a precise determination of nuclear charge radius differences.

In addition to the Na-like calculation presented in Ref. [23], we have now achieved calculation of the significantly more complicated Mg-like transition energies. The strong state mixing within the $n = 3$ complex necessitates a hybrid RMBPT and configuration interaction approach of constructing an effective Hamiltonian within the $n = 3$ subspace, including QED effects. This Hamiltonian is then diagonalized. Transition energies of the corresponding Na-like ions appear on the diagonal as valence-core interaction terms, while Mg-like-specific valence-valence interactions contribute to both diagonal and off-diagonal elements. A term representing the Ne-like core energy cancels in transition energy differences, simplifying the computation and improving accuracy. Further details of the method and classification of RMBPT and QED contributions can be found in Ref. [27] and in our companion paper [28].

Nuclear Structure Theory — The experimental results are compared with predictions from nuclear DFT. We consider two kinds of energy density functionals: the widely used Skyrme functional [29] and the Fayans functional [30, 31] which has nonstandard surface and pairing terms containing gradient couplings. Specifically, we use the Skyrme functional strong state mixing SV-min [32] and the Fayans functionals Fy(Δr , HFB) [33] and Fy(IPV) [34]. All three parametrizations have been calibrated to the same set of nuclear observables from Ref. [32]. The Fy(Δr , HFB) calibration dataset additionally incorporates selected differential charge-radius data from the Ca isotopic chain. The dataset of Fy(IPV) also contains selected charge radii differences along the semimagic Sn and Pb isotopic chains, and employs more general isospin-dependent pairing term. The uncertainties of the calibrated model parameters are propagated to calculated observables, such as charge radii, by means of the linear regression technique [32, 35]. Odd- A nuclei are computed with the blocking method [3], by identifying one-quasiparticle configurations of odd nucleons through

their quantum numbers: angular momentum projection on the symmetry axis and parity. The charge radii were computed from charge densities containing relativistic corrections (Darwin and spin-orbit term) and contributions from intrinsic nucleonic electric and magnetic form factors [36]. Further details are included in our companion paper [28].

Scaled Radius Difference — Our core idea is to constrain the allowable set of nuclear charge radii by requiring that the theoretical transition-energy difference, $E_B^T(R_B) - E_A^T(R_A)$, equals the experimentally measured difference, $E_B^M - E_A^M$, for two nuclides A and B. Theoretical transition energies are well approximated by a linear expansion around some reference charge radius R_0 [23]. The primary observable is the scaled radius difference

$$D_{BA} \equiv R_B - \frac{S_A}{S_B} R_A = [E_B^M - E_A^M] / S_B - [E_B^T(R_{B_0}) - E_A^T(R_{A_0})] / S_B + \left[R_{B_0} - \frac{S_A}{S_B} R_{A_0} \right], \quad (1)$$

where $S_A \equiv \partial E_A / \partial R_A$ and $S_B \equiv \partial E_B / \partial R_B$ are the nuclear sensitivity coefficients [27].

In earlier analyses [23, 37], Eq. (1) was solved for the charge radius of a target isotope R_B using a reference isotope R_A as an anchor. The scaled radius difference removes dependence on an arbitrarily chosen reference isotope and provides a clear representation of the experimental constraint (see Fig. 1).

Experimental Details — The measurements were carried out at the Tokyo Electron Beam Ion Trap (EBIT) [38, 39], operated at 10 keV electron beam energy and 100 mA beam current. Lu and Yb atoms were injected into the trap using a Knudsen cell source [40, 41], while Ne and W were co-injected to provide reference lines for wavelength calibration. Extreme ultraviolet spectra of trapped ions were recorded with a flat-field grazing-incidence spectrometer [42] equipped with a cooled CCD detector, achieving a resolution of 0.01 nm. Both Na-like and Mg-like charge states were studied, providing independent and complementary sensitivity to the nuclear charge radius. A time-dependent wavelength calibration corrected for spectrometer drift, and all measurements of Lu, Yb, and calibration elements were interleaved to ensure identical EBIT conditions. Further details of ion injection, spectrometer operation, and data processing are given in the companion paper [28].

Data Analysis — Experimentally, the analysis of the extreme ultraviolet spectra focused on extracting the shift in Na-like $3p^2 P_{1/2} \rightarrow 3s^2 S_{1/2}$ and Mg-like $3s3p^3 P_1 \rightarrow 3s^2 1S_0 D_1$ transition energies from our measured spectra. The data recorded were processed using a combination of image correction, spectral fitting, and wavelength calibration techniques.

Raw CCD images included a slight tilt of the spectral lines, occasional cosmic ray hits, and background signal from stray light. Line tilt was corrected by rotating

the images, while cosmic ray artifacts were removed using contour detection algorithms, ensuring clean spectra for subsequent analysis. For the background, we implemented a flat-field correction technique based on a sliding minimum filter [28].

Spectral lines were fit using a Gaussian profile superimposed on a constant background, typically within a narrow window of ± 8 pixels around the peak. Calibration was performed using well-known Ne and W emission lines. A time-dependent calibration model was implemented which allowed for a linear drift in time over the course of each day, but with a shared spatial dispersion for all days. To assist in determining the time drift, a term in the calibration loss function was added that penalized spread in the calculated wavelengths of the Na- and Mg-like transitions of Lu and Yb.

The Lu-Yb D_1 transition energy shifts in each injection session were extracted for both Na-like and Mg-like charge states. Both the calibration of the spectrometer and the line statistics contribute to the experimental shift uncertainties. To account for any unresolved systematic uncertainties, all experimental uncertainties were multiplied by the square root of our calibration χ^2_ν [43]. These experimentally determined energy differences were then compared to theoretical predictions from our relativistic many-body perturbation theory calculations [23, 27].

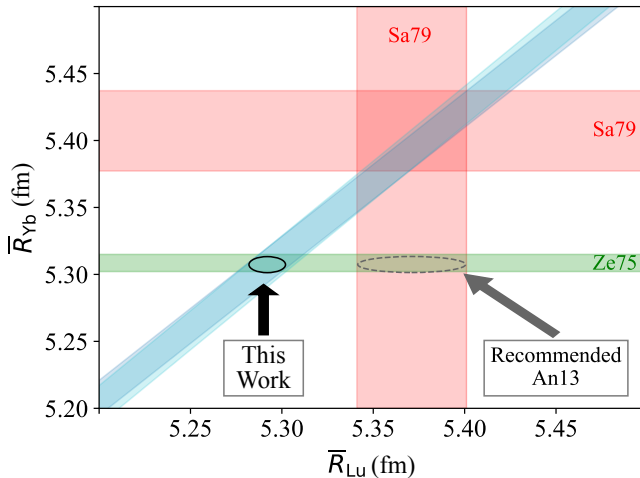


FIG. 1. 1- σ constraints placed on the joint probability distribution of naturally abundant Yb and Lu. Previous absolute measurements from electron scattering (Sa79: [25]) and muonic atom spectroscopy (Ze75: [24]) are displayed in red and green bands, respectively. The 1- σ confidence region from [26] is shown by the dashed ellipse. The highly charged ions constraints from this work are shown in blue (blue for Na-like, cyan for Mg-like) with the combined result of our result and Ze75 shown by a black ellipse.

Results — In this work, we use natural-abundance samples. We denote the abundance-weighted average radius as $\bar{R}_A = \sum_i w_i R_{iA}$, and the corresponding abundance-weighted scaled radius difference as \bar{D}_{BA} .

Details, including the averaging over natural isotopic abundances, improved treatment of higher-order nuclear moments, and the statistical combination of our result with other measurements, are provided in the companion paper [28].

We determined the scaled radius difference between Yb and Lu by combining experimentally measured Na-like and Mg-like energy differences with theoretical transition energy separations. The experimental differences are

$$E_{\text{Lu}}^{M,\text{Na}} - E_{\text{Yb}}^{M,\text{Na}} = 3.235(3) \text{ eV},$$

$$E_{\text{Lu}}^{M,\text{Mg}} - E_{\text{Yb}}^{M,\text{Mg}} = 3.229(3) \text{ eV},$$

while the corresponding theoretical separations, calculated using reference radii $\bar{R}_{\text{Yb}_0} = 5.3051$ fm and $\bar{R}_{\text{Lu}_0} = 5.3701$ fm, obtained as natural-abundance averages from Ref. [26], are

$$E_{\text{Lu}}^{T,\text{Na}}(\bar{R}_{\text{Lu}_0}) - E_{\text{Yb}}^{T,\text{Na}}(\bar{R}_{\text{Yb}_0}) = 3.2144(6) \text{ eV},$$

$$E_{\text{Lu}}^{T,\text{Mg}}(\bar{R}_{\text{Lu}_0}) - E_{\text{Yb}}^{T,\text{Mg}}(\bar{R}_{\text{Yb}_0}) = 3.2103(7) \text{ eV}.$$

By comparing these experimental and theoretical values, we extracted the scaled difference in nuclear radii between Yb and Lu. With these results, the constraints we place on the scaled radius differences are:

$$\bar{D}_{\text{Lu},\text{Yb}}^{\text{Na}} = 0.535(12) \text{ fm}, \bar{D}_{\text{Lu},\text{Yb}}^{\text{Mg}} = 0.540(13) \text{ fm}. \quad (2)$$

For visualization purposes, these constraints are presented in Fig. 1, along with the muonic atom spectroscopy and elastic electron scattering results described in [28]. These measurements were converted to a natural-abundance averaged equivalent using the abundances of [44] and the optical isotope shift studies of [45] and [46–50].

Adopting the Yb radii from the evaluations of Refs. [26] and [51], we obtain a ^{175}Lu radius of 5.291(11) fm and an isotonic difference of $R_{^{175}\text{Lu}} - R_{^{174}\text{Yb}} = -0.017(10)$ fm.

Discussion and Conclusions — Our measurement of the $^{175}\text{Lu} - ^{174}\text{Yb}$ scaled nuclear charge radius difference provides a unique constraint on the charge radius surface and resolves a longstanding anomaly in the rare-earth region. The Mg-like calculations, along with our improved handling of higher order nuclear moments, extraction of the scaled nuclear radius difference, and tools for a generalized least squares analysis of all measurements, provide a rigorous framework to interpret future highly charged ion radius results. The radius constraints from the Na-like and Mg-like D_1 line energies agree with each other, supporting the accuracy of the Mg-like transition energy calculation and allowing for a reduction in statistical uncertainties.

The extracted isotonic difference $R_{^{175}\text{Lu}} - R_{^{174}\text{Yb}}$ diverges from the recommended values [26, 51] that had suggested an inversion of the expected odd-even staggering pattern for the Yb-Lu-Hf triplet. In contrast, our

result displays a similar decrease in isotonic radius from Yb to Lu as observed in previous elastic electron scattering work [25]. This, combined with the disagreement between electron scattering and muonic atom results, suggests a common systematic effect that affects both radii from [25].

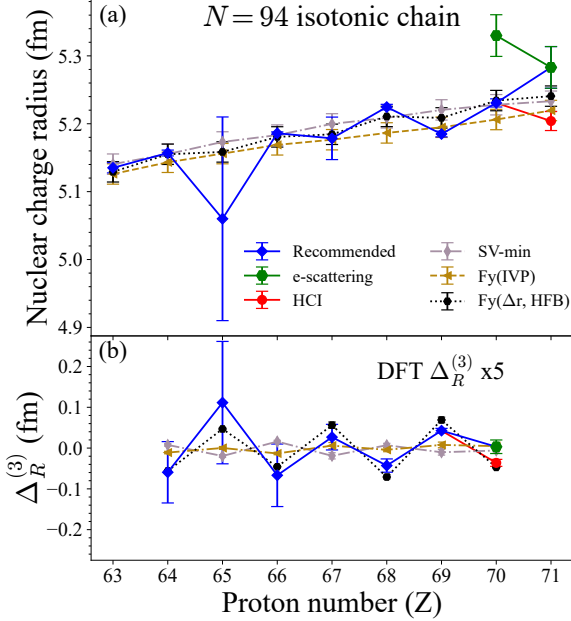


FIG. 2. (a) Charge radii along the $N = 94$ isotonic chain. The recommended values are anchored mostly by muonic atom spectroscopy [26, 52], with the exception of $R_{160}\text{Dy}$, which was taken from [51] due to an apparent overestimation of uncertainty in [26]; they include the measurement from this work (solid red circles) alongside electron-scattering data [25] for $Z = 70\text{--}71$ (green hexagons). Nuclear DFT predictions using Skyrme (SV-min) and Fayans (Fy(IPV), Fy(Δr ,HFB)) functionals are also shown. (b) The corresponding OESR (3). The calculated values of OESR and their uncertainties are multiplied by five for the sake of visibility.

For the sake of comparison with nuclear DFT calculations, we extracted the experimental nuclear charge radii for the long $N = 94$ isotonic chain from [26] and included $R_{165}\text{Lu}$ from our current result, see Fig. 2(a). In the calculations, we assumed the experimental assignments for the one-quasiproton states in odd- Z nuclei with the corresponding Nilsson labels [53]: [413]5/2 $^{+}$ for ^{157}Eu , [411]3/2 $^{+}$ for ^{159}Tb , [523]7/2 $^{-}$ for ^{161}Ho , [411]1/2 $^{+}$ for ^{163}Tm , and [404]7/2 $^{+}$ for ^{165}Lu . This sequence of one-quasiproton band-heads is reproduced by theory [8], except for the inverted ordering of the close-lying [523]7/2 $^{-}$ and [411]1/2 $^{+}$ levels at $Z = 67$ and $Z = 69$.

Figure 2(b) shows the OESR of charge radii (OESR):

$$\Delta_R^{(3)} = \frac{1}{2} (R_{N+1} - 2R_N + R_{N-1}). \quad (3)$$

Theoretically, the OESR is primarily influenced by nucleonic pairing and quadrupole polarization effects, see,

e.g., Refs. [10, 17, 54–57]. In particular, the pairing effect is the main source of the OESR in spherical semi-magic nuclei. Strong deformation effects in OESR have been seen in transitional nuclei that are deformation-soft, in which an odd nucleon in a deformation-driven orbital can significantly polarize the nuclear shape [57]. For well deformed nuclei, such as those investigated in this work, such shape-polarization effect are considerably weaker [53].

In general, the charge radii recommended in [26] are fairly well reproduced by our DFT models, considering experimental and theoretical uncertainties. While DFT calculations reproduce the absolute charge radius of ^{165}Lu inferred from our $R_{175}\text{Lu}$ result, all models predict a much smaller OESR than both the currently recommended values [26] and our result. As discussed in the companion paper [28], we found the OESR in the calculated pairing energy and quadrupole deformation to be weak along the $N = 94$ sequence, which is consistent with the weaker predicted OESR.

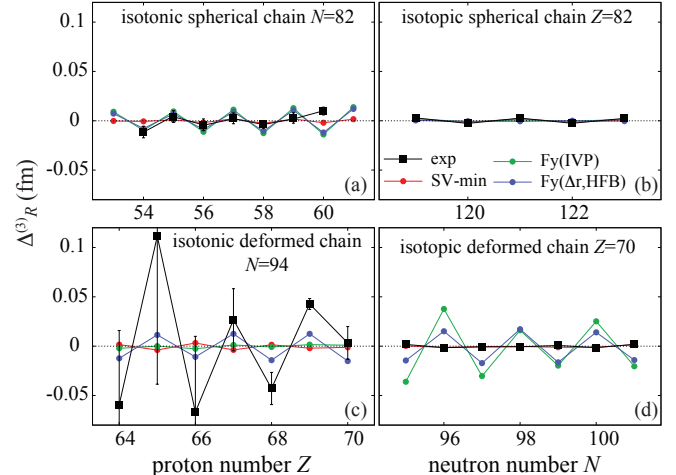


FIG. 3. DFT predictions and experimental recommended values [26] for $\Delta_R^{(3)}$ in isotonic (left) and isotopic (right) chains of selected spherical (top) and deformed (bottom) nuclei. Note the dramatic change of the experimental OESR magnitude for the deformed $N = 94$ chain when compared to other cases.

To get a better insight into discrepancy seen in Fig. 2(b), Fig. 3 shows experimental and theoretical values of $\Delta_R^{(3)}$ for isotonic $N = 82$ and 94 and isotopic $Z = 82$ and 70 chains. The semi-magic nuclei with $Z = 82$ or $N = 82$ are spherical while the rare-earth chains are strongly deformed. The DFT calculations reproduce OESR for spherical sequences, as well as for the deformed Yb isotopic chain, with the model dependence of the predicted magnitude of OESR being primarily attributed to different pairing functionals employed [28]. For the $N = 94$ nuclei, the experimental OESR is very large: it exceeds the experimental OESR values in other sequences displayed by a factor of ≈ 30 . The calculated OESR values are consistent with the data for the de-

formed Yb chain, and hence do not offer any explanation for the enhancement seen in the recommended $N = 94$ values.

Improving the precision of the Tb and Ho charge radii, or equivalently their radius difference relative to Dy ($Z = 66$), would provide useful insight into whether the pronounced experimental OESR seen Fig. 2 is statistical or systematic. Given the complexity of muonic-atom spectra in the highly deformed region $60 \leq Z \leq 77$ [26], highly charged ion spectroscopy could provide a particularly powerful approach for establishing radius trends in this region.

Acknowledgments — This work was funded by a NIST Grant Award Number 70NANB20H87 and by a National Science Foundation Award Number 2309273. It was also supported by the U.S. Department of Energy under Award Number DE-SC0013365 (Office of Science, Office of Nuclear Physics) and DE-SC0023175 (Office of Science, NUCLEI SciDAC-5 collaboration). E.T. gratefully acknowledges the kind hospitality of the research groups at the National Institute for Fusion Science and the University of Electro-Communications during the course of this work.

[1] S. D. Drell, Nuclear radius and nuclear forces, *Phys. Rev.* **100**, 97 (1955).

[2] A. Bohr and B. R. Mottelson, *Nuclear Structure, vol. I* (W. A. Benjamin, New York, 1969).

[3] P. Ring and P. Schuck, *The nuclear many-body problem* (Springer-Verlag, Berlin, 1980).

[4] A. Ekström, G. R. Jansen, K. A. Wendt, G. Hagen, T. Papenbrock, B. D. Carlsson, C. Forssén, M. Hjorth-Jensen, P. Navrátil, and W. Nazarewicz, Accurate nuclear radii and binding energies from a chiral interaction, *Phys. Rev. C* **91**, 051301 (2015).

[5] P.-G. Reinhard and W. Nazarewicz, Nuclear charge and neutron radii and nuclear matter: Trend analysis in skyrme density-functional-theory approach, *Phys. Rev. C* **93**, 051303 (2016).

[6] W. Nörtershäuser and I. D. Moore, Nuclear charge radii, in *Handbook of Nuclear Physics*, edited by I. Tanihata, H. Toki, and T. Kajino (Springer Nature Singapore, Singapore, 2023) pp. 243–312.

[7] T. Miyagi, Nuclear radii from first principles, *Front. Phys.* **13**, May (2025).

[8] P.-G. Reinhard and W. W. Nazarewicz, Statistical Correlations of Nuclear Quadrupole Deformations and Charge Radii, *Phys. Rev. C* **106**, 014303 (2022).

[9] S. Zerguine, P. Van Isacker, and A. Bouldjedri, Consistent description of nuclear charge radii and electric monopole transitions, *Phys. Rev. C* **85**, 034331 (2012).

[10] S. Geldhof, M. Kortelainen, O. Beliuskina, P. Campbell, L. Caceres, L. Cañete, B. Cheal, K. Chrysalidis, C. S. Devlin, R. P. de Groote, *et al.*, Impact of nuclear deformation and pairing on the charge radii of palladium isotopes, *Phys. Rev. Lett.* **128**, 152501 (2022).

[11] J. Warbinek, E. Rickert, S. Raeder, T. Albrecht-Schönzart, B. Andelic, J. Auler, B. Bally, M. Bender, S. Berndt, M. Block, *et al.*, Smooth trends in fermium charge radii and the impact of shell effects, *Nature* **634**, 1075 (2024).

[12] J. Hur, D. P. L. Aude Craik, I. Counts, E. Knyazev, L. Caldwell, C. Leung, S. Pandey, J. C. Berengut, A. Geddes, W. Nazarewicz, *et al.*, Evidence of two-source king plot nonlinearity in spectroscopic search for new boson, *Phys. Rev. Lett.* **128**, 163201 (2022).

[13] M. Door, C.-H. Yeh, M. Heinz, F. Kirk, C. Lyu, T. Miyagi, J. C. Berengut, J. Bieroń, K. Blaum, L. S. Dreissen, *et al.*, Probing new bosons and nuclear structure with ytterbium isotope shifts, *Phys. Rev. Lett.* **134**, 063002 (2025).

[14] Z. Sun, K. A. Beyer, Z. A. Mandrykina, I. A. Valuev, C. H. Keitel, and N. S. Oreshkina, ^{208}Pb nuclear charge radius revisited: Closing the fine-structure-anomaly gap, *Phys. Rev. Lett.* **135**, 163002 (2025).

[15] K. A. Beyer, T. E. Cocolios, C. Costache, M. Deseyn, P. Demol, A. Doinaki, O. Eizenberg, M. Gorshteyn, M. Heines, A. Herzáñ, *et al.*, *Modern approach to muonic X-Ray spectroscopy demonstrated through the measurement of stable Cl radii* (2025), 2506.08804 [nucl-ex].

[16] R. F. Garcia Ruiz, M. L. Bissell, K. Blaum, A. Ekström, N. Frömmgen, G. Hagen, M. Hammen, K. Hebeler, J. D. Holt, G. R. Jansen, *et al.*, Unexpectedly large charge radii of neutron-rich calcium isotopes, *Nat. Phys.* **12**, 594 (2016).

[17] R. P. de Groote, J. Billowes, C. L. Binnersley, M. L. Bissell, T. E. Cocolios, T. D. Goodacre, G. J. Farooq-Smith, D. V. Fedorov, K. T. Flanagan, S. Franchoo, *et al.*, Measurement and Microscopic Description of Odd–Even Staggering of Charge Radii of Exotic Copper Isotopes, *Nat. Phys.* **16**, 620 (2020).

[18] S. V. Pineda, K. König, D. M. Rossi, B. A. Brown, A. Incorvati, J. Lantis, K. Minamisono, W. Nörtershäuser, J. Piekariewicz, R. Powel, and F. Sommer, Charge radius of neutron-deficient ^{54}Ni and symmetry energy constraints using the difference in mirror pair charge radii, *Phys. Rev. Lett.* **127**, 182503 (2021).

[19] P.-G. Reinhard and W. Nazarewicz, Information content of the differences in the charge radii of mirror nuclei, *Phys. Rev. C* **105**, L021301 (2022).

[20] P. Bano, S. P. Pattnaik, M. Centelles, X. Viñas, and T. R. Routray, Correlations between charge radii differences of mirror nuclei and stellar observables, *Phys. Rev. C* **108**, 015802 (2023).

[21] S. J. Novario, D. Lonardoni, S. Gandolfi, and G. Hagen, Trends of neutron skins and radii of mirror nuclei from first principles, *Phys. Rev. Lett.* **130**, 032501 (2023).

[22] B. Ohayon, Critical evaluation of reference charge radii and applications in mirror nuclei, *At. Data Nucl. Data Tables* **165**, 101732 (2025).

[23] A. Hosier, Dipti, S. A. Blundell, A. Lapierre, R. Silwal, G. Gwinnier, J. N. Tan, A. Naing, J. D. Gillaspy, Y. Yang, *et al.*, Determination of nuclear charge radius by extreme-ultraviolet spectroscopy of Na-like ions, *Phys. Rev. Res.* **7**, L012024 (2025).

[24] A. Zehnder, F. Boehm, W. Dey, R. Engfer, H. Walter, and J. Vuilleumier, Charge parameters, isotope shifts, quadrupole moments, and nuclear excitation in muonic $170\text{--}174,176\text{-Yb}$, *Nucl. Phys. A* **254**, 315 (1975).

[25] T. Sasanuma, *Electron Scattering from Deformed Heavy Nuclei*, Ph.d. thesis, Massachusetts Institute of Technology (1979).

[26] I. Angeli and K. P. Marinova, Table of experimental nuclear ground state charge radii: An update, *At. Data Nucl. Data Tables* **99**, 69 (2013).

[27] J. D. Gillaspy, D. Osin, Y. Ralchenko, J. Reader, and S. A. Blundell, Transition energies of the D lines in Na-like ions, *Phys. Rev. A* **87**, 062503 (2013).

[28] H. Staiger, E. Takacs, S. Blundell, N. Kimura, H. Sakaue, R. Garcia Ruiz, W. Nazarewicz, P.-G. Reinhard, C. Faiyaz, C. Suzuki, *et al.*, Extreme Ultraviolet Spectroscopy of Highly Charged Lu and Yb Ions for Nuclear Charge Radius Determination, arXiv preprint arXiv:2511.20537 (2025), [arXiv:2511.20537 \[physics.atom-ph\]](https://arxiv.org/abs/2511.20537).

[29] M. Bender, P.-H. Heenen, and P.-G. Reinhard, Self-consistent mean-field models for nuclear structure, *Rev. Mod. Phys.* **75**, 121 (2003).

[30] S. A. Fayans, Towards a universal nuclear density functional, *J. Exp. Theor. Phys. Lett.* **68**, 169 (1998).

[31] S. A. Fayans, S. V. Tolokonnikov, E. L. Trykov, and D. Zawischa, Nuclear isotope shifts within the local energy-density functional approach, *Nucl. Phys. A* **676**, 49 (2000).

[32] P. Klüpfel, P.-G. Reinhard, T. J. Bürvenich, and J. A. Maruhn, Variations on a theme by Skyrme: A systematic study of adjustments of model parameters, *Phys. Rev. C* **79**, 034310 (2009).

[33] A. J. Miller, K. Minamisono, A. Klose, D. Garand, C. Kujawa, J. D. Lantis, Y. Liu, B. Maaß, P. F. Mantica, W. Nazarewicz, *et al.*, Proton superfluidity and charge radii in proton-rich calcium isotopes, *Nat. Phys.* **15**, 432 (2019).

[34] J. Karthein, C. Ricketts, R. Garcia Ruiz, J. Billowes, C. Binnersley, T. Cocolios, J. Dobaczewski, G. Farooq-Smith, K. Flanagan, G. Georgiev, *et al.*, Electromagnetic properties of indium isotopes elucidate the doubly magic character of ^{100}Sn , *Nat. Phys.* (2023).

[35] J. Dobaczewski, W. Nazarewicz, and P.-G. Reinhard, Error estimates of theoretical models: a guide, *J. Phys. G* **41**, 074001 (2014).

[36] P.-G. Reinhard and W. Nazarewicz, Nuclear charge densities in spherical and deformed nuclei: Toward precise calculations of charge radii, *Phys. Rev. C* **103**, 054310 (2021).

[37] A. Hosier, Dipti, S. A. Blundell, R. Silwal, A. Lapierre, J. D. Gillaspy, G. Gwinnier, J. N. Tan, A. A. Kwiatkowski, Y. Wang, *et al.*, Absolute nuclear charge radius by Na-like spectral line separation in high-Z elements, *J. Phys. B: At. Mol. Opt. Phys.* **57**, 195001 (2024).

[38] F. J. Currell, J. Asada, K. Ishii, A. Minoh, K. Motohashi, N. Nakamura, K. Nishizawa, S. Ohtani, K. Okazaki, M. Sakurai, *et al.*, A new versatile electron-beam ion trap, *J. Phys. Soc. Jpn.* **65**, 3186 (1996).

[39] N. Nakamura, J. Asada, F. J. Currell, T. Fukami, T. Hirayama, K. Motohashi, T. Nagata, E. Nojikawa, S. Ohtani, K. Okazaki, *et al.*, An overview of the Tokyo electron beam ion trap, *Phys. Scr.* **1997**, 362 (1997).

[40] C. Yamada, K. Nagata, N. Nakamura, S. Ohtani, S. Takahashi, T. Tobiayama, M. Tona, H. Watanabe, N. Yoshiyasu, M. Sakurai, *et al.*, Injection of metallic elements into an electron-beam ion trap using a knudsen cell, *Rev. Sci. Instrum.* **77**, 066110 (2006).

[41] N. Nakamura, T. Kinugawa, H. Shimizu, H. Watanabe, S. Ito, S. Ohtani, C. Yamada, K. Okazaki, M. Sakurai, M. R. Tarbutt, *et al.*, Injection of various metallic elements into an electron beam ion trap: Techniques needed for systematic investigations of isoelectronic sequences, *Rev. Sci. Instrum.* **71**, 684 (2000).

[42] H. Ohashi, J. Yatsurugi, H. A. Sakaue, and N. Nakamura, High resolution extreme ultraviolet spectrometer for an electron beam ion trap, *Rev. Sci. Instrum.* **82**, 083103 (2011).

[43] R. T. Birge, The calculation of errors by the method of least squares, *Phys. Rev.* **40**, 207 (1932).

[44] M. Berglund and M. E. Wieser, Isotopic compositions of the elements 2009 (IUPAC Technical Report), *Pure and Applied Chemistry* **83**, 397 (2011).

[45] U. Georg, W. Borchers, M. Keim, A. Klein, P. Lievens, R. Neugart, M. Neuroth, P. M. Rao, C. Schulz, and the ISOLDE Collaboration, Laser spectroscopy investigation of the nuclear moments and radii of lutetium isotopes, *Eur. Phys. J. A* **3**, 225 (1998).

[46] A. E. Barzakh, I. Y. Chubukov, D. V. Fedorov, F. V. Moroz, V. N. Panteleev, M. D. Seliverstov, and Y. M. Volkov, Isotope shift and hyperfine structure measurements for 155-Yb by laser ion source technique, *Eur. Phys. J. A* **1**, 3 (1998).

[47] A. E. Barzakh, I. Y. Chubukov, D. V. Fedorov, V. N. Panteleev, M. D. Seliverstov, and Y. M. Volkov, Mean square charge radii of the neutron-deficient rare-earth isotopes in the region of the nuclear shell $N \approx 82$ measured by the laser ion source spectroscopy technique, *Phys. Rev. C* **61**, 034304 (2000).

[48] C. Schulz, E. Arnold, W. Borchers, W. Neu, R. Neugart, M. Neuroth, E. W. Otten, M. Scherf, K. Wendt, P. Lievens, *et al.*, Resonance ionization spectroscopy on a fast atomic ytterbium beam, *Journal of Physics B: Atomic, Molecular and Optical Physics* **24**, 4831 (1991).

[49] W.-G. Jin, T. Horiguchi, M. Wakasugi, T. Hasegawa, and W. Yang, Systematic study of isotope shifts and hyperfine structures in Yb I by atomic-beam laser spectroscopy, *J. Phys. Soc. Japan* **60**, 2896 (1991).

[50] G. D. Sprouse, J. Das, T. Lauritsen, J. Schecker, A. Berger, J. Billowes, C. H. Holbrow, H.-E. Mahnke, and S. L. Rolston, Laser spectroscopy of light Yb isotopes on-line in a cooled gas cell, *Phys. Rev. Lett.* **63**, 1463 (1989).

[51] G. Fricke and K. Heilig, *Nuclear Charge Radii*, edited by H. Schopper (Springer Materials, 2004).

[52] I. Angeli, *Table of Nuclear Root Mean Square Charge Radii*, Tech. Rep. INDC(HUN)-033 (IAEA Nuclear Data Section, 1999) available at <http://www-nds.iaea.org/at/indc-se1.html>.

[53] W. Nazarewicz, M. Riley, and J. Garrett, Equilibrium deformations and excitation energies of single-quasiproton band heads of rare-earth nuclei, *Nucl. Phys. A* **512**, 61 (1990).

[54] P.-G. Reinhard and W. Nazarewicz, Toward a global description of nuclear charge radii: Exploring the fayans energy density functional, *Phys. Rev. C* **95**, 064328 (2017).

[55] Á. Koszorús, X. F. Yang, W. G. Jiang, S. J. Novario, S. W. Bai, J. Billowes, C. L. Binnersley, M. L. Bissell, T. E. Cocolios, B. S. Cooper, *et al.*, Charge radii of exotic potassium isotopes challenge nuclear theory and the magic character of $n = 32$, *Nat. Phys.* **17**, 439 (2021).

- [56] F. Le Blanc, D. Lunney, J. Obert, J. Oms, J. C. Putaux, B. Roussi  re, J. Sauvage, S. Zemlyanoi, J. Pinard, Cabaret, *et al.* (ISOLDE Collaboration), Large odd-even radius staggering in the very light platinum isotopes from laser spectroscopy, *Phys. Rev. C* **60**, 054310 (1999).
- [57] B. A. Marsh, T. Day Goodacre, S. Sels, Y. Tsunoda, B. Andel, A. N. Andreyev, N. A. Althubiti, D. Atanasov, A. E. Barzakh, J. Billowes, *et al.*, Characterization of the shape-staggering effect in mercury nuclei, *Nat. Phys.* **14**, 1163 (2018).